Catal Lett (2007) 118:224–230
DOI 10.1007/s10562-007-9174-x

Enhancing Effects of Ultrasound Treatment on the Preparation of TiO_2 Photocatalysts

Sung-Yeon Kim · Tae-Sun Chang · Chae-Ho Shin

Received: 3 April 2007 / Accepted: 17 June 2007 / Published online: 17 July 2007

Abstract TiO_2 nanoparticles were synthesized by the hydrolysis and condensation of $TiCl_4$ in a mixed solvent of iso-propyl alcohol and water with or without ultrasound treatment. As-prepared powders were characterized by X-ray diffraction (XRD), field emission scanning electron microscopy (FE-SEM), energy filtering transmission electron microscopy (EF-TEM), particle size analysis and BET surface area analysis. The specific surface area, thermal stability and crystallization of the as-prepared samples treated with ultrasound were higher than those of samples treated without ultrasound. To examine the photocatalytic activity of the as-prepared TiO_2, the photodegradation of MB which is a typical dye resistant to biodegradation has been investigated on TiO_2 powders in aqueous heterogeneous suspensions. The photocatalytic degradation of a aqueous solution of methylene blue shows a remarkable increase when it is carried out with ultrasound in all cases.

Keywords TiO_2 · Photoactivity · Methylene blue · Ultrasound · $TiCl_4$

1 Introduction

TiO_2 has a variety of functional applications ranging from pigments to photoconductors, sensor materials and dielectric ceramics. The material has also been studied extensively in recent years as a photocatalyst to deal with environmental pollution, water purification, wastewater treatment, hazardous waste control and air purification. The photocatalytic activity of TiO_2 nanoparticle is greatly influenced by its crystal structure, particle size, surface are and porosity. When the size of TiO_2 particle is decreased to nanometer scale, the catalytic activity is enhanced because the optical band gap is widened due to the quantum size effect, combined with the increased surface area [1]. Titania has three different crystalline phases; rutile, anatase and brookite, among which rutile is in the thermodynamically stable state while the latter two phases are in the metastable state. Various kinds of methods including the sol–gel method [2], vapor decomposition of titanium alkyloxides or $TiCl_4$ in oxygen [3, 4], the hydrothermal technique [5], the reversed micelle method titania nanostructures [6], and oxidation of metallic Ti powder [7] were used to prepare titania nanostructures. The sol–gel method is widely used to prepare nanometer TiO_2, but the precipitates derived by sol–gel are amorphous in nature, and require further treatment to induce crystallization. The hydrothermal technique is widely employed to enhance crystallization at both laboratory and commercial scales. However, many factors, reaction temperature, reaction time, type of precursor and the medium, may influence the crystallization process. In contrast, the ultrasound treatment, by which powerful ultrasound is used to stimulate chemical processes in liquids, has become an important tool in nanocrystalline synthesis in recent years since it is easy to carry out and causes novel chemical reactions and physical changes which do not occur in ambient environment [8]. When solutions are exposed to strong ultrasound treatment, bubbles are implosively collapsed by acoustic

S.-Y. Kim · C.-H. Shin (✉)
Department of Chemical Engineering, Chungbuk National University, Cheongju, Chungbuk 361-763, Korea
e-mail: chshin@chungbuk.ac.kr

T.-S. Chang (✉)
Advanced Chemical Technology Division, Korea Research Institute of Chemical Technology, Daejeon 350-343, Korea
e-mail: tschang@krict.re.kr

fields in the solution. High-temperature and high-pressure fields are produced at the center of the bubbles. The collapse of bubbles generates localized hot spots with transient temperatures of about 5000 K, pressures of about 500atm, and heating and cooling rates greater than 109 K/s. This effect is known as acoustic cavitation. More uniform dispersion of the nanoparticles, higher surface area, better thermal stability and phase purity are some of the advantages of ultrasonication method [9]. Now, nanostuctured metals, alloys, oxides, carbides and sulfides, or nanometer colloids, nanostructure-supported catalysts and biomaterials can all be prepared by using high intensive ultrasound method [10].

In this work, TiO_2 nanoparticles were synthesized by the ultrasound treatment. And the effect of ultrasound treatment on the crystalline and morphology of the products were investigated. The behavior of titania in photocatalytic decomposition of methylene blue in aqueous solution was studied. This method is suitable for the deposition on various substrates at relative economic treatment.

2 Experimental

2.1 Preparation of Nano-Sized Titanium dioxide Powders

The preparation of nano-sized titanium dioxide was carried out using a sol-hydrothermal method of titanium tetrachloride (Extra pure grade, $TiCl_4$, Yakuri Pure Chemicals Co., Japan), which was used as a starting material without any further purification. $TiCl_4$ was dissolved in deionized water maintaining at 4 °C to avoid rapid precipitation. The concentration of titanium was adjusted to 0.5 M. The aqueous solution was mixed with mixed solvent of isopropyl alcohol and water with a volume ratio of 2. The aqueous solution was vigorously stirred for 4 h at room temperature. This solution was treated by two methods. One handles without ultrasound treatment, and the other handles with ultrasound treatment. In case of ultrasound treatment, the solution was treated (branson sonifier 450, 80 W) for 30 min and aged at 70 °C for 1 h to carry out hydrothermal hydrolysis and then white precipitate was formed. After precipitation, the solution was neutralized with a 2% NH_4OH solution adding dropwise in order to remove chloride ions. The precipitate was separated by filtration and washing three times with deionized water, and finally rinsed with acetone. The obtained precipitate was aged in an autoclave at 200 °C for 2 h and then dried in air at 80 °C over night. The oven-dried gels were calcined at 400, 500, 600, 700, 800 and 900 °C for 2 h in open-air atmosphere.

2.2 Characterization

Powder X-ray diffraction (XRD) patterns were collected on a D/MAX-IIIB diffractometer with CuK_α radiation at 40 kV and 40 mA. XRD was used for crystal phase, estimation of the anatase-to-rutile ratio and the particle size of each phase present [11]. The crystallite sizes were determined from corresponding X-ray spectral peaks by the Scherrer equation ($\alpha = 0.89\lambda/B_{1/2}\cos\theta$, λ = wavelength of incident X-ray; $B_{1/2}$ = width of half high peak; θ = diffraction angle) using the peak of the anatase (101) at $2\theta = 25.35$ ° and the rutile (110) at 27.45°.

The morphologies of the synthesized samples were conducted on Jeol JSM-6700F field emission scanning electron microscope (FE-SEM) and Carl Zeiss EM 912 Omega energy filtering transmission electron microscope (EF-TEM). The samples were dispersed in absolute ethanol and sonicated ultrasonically to separate out individual particles for the determination of particle size.

A particle size analyzer (Bi-DCP particle sizer) was used to measure particle size and particle distribution of the prepared powders.

BET surface area and total pore volume were measured by nitrogen adsorption-desorption isotherms at 77 K with a Micromeritics ASAP 2010 nitrogen adsorption apparatus.

2.3 Photodegradation of MB

In order to examine the photocatalytic activity of TiO_2 prepared, the photodegradation of MB blue has been investigated in aqueous heterogeneous suspensions equipped with UV radiation source. A biannular quartz glass reactor with the lamp immersed in the inner part was used for all photocatalytic experiments. In a MB aqueous solution of 1,000 mL with a concentration of 0.05 mM of MB, sample powders of 0.3 g were dispersed under ultrasonic vibration for 5 min. A 9 W black light blue lamp (Philips, PLS9W/08.BLB) was used as the UV radiation source. All experiments were conducted at room temperature without a supply of air.

The samples were centrifuged to separate the TiO_2 from the solution, and the absorption was measured at 665 nm of the remained solution [12, 13]. The absorption was converted to relative concentration of MB (C/C_0) referring to a standard curve and displayed linear behavior between relative concentration and the absorption at this wavelength.

3 Results and Discussion

Figure 1 shows the x-ray diffraction patterns of the TiO_2 nanoparticles calcined at different temperatures. The calcination temperatures that begin to change from amorphous

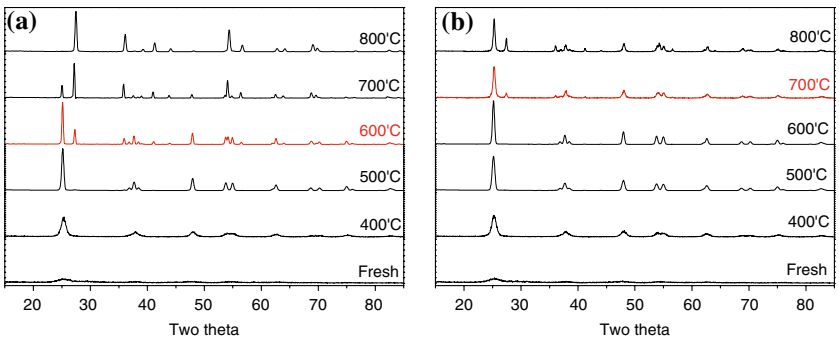

Fig. 1 XRD powder patterns of the as-prepared samples calcined at different temperature under flowing air: without ultrasonic treatment (**a**), with ultrasonic treatment (**b**)

structure to anatase structure and from anatase structure to rutile structure differ in samples prepared. The sample treated without ultrasound begins to appear rutile structure from more than 600 °C. At this temperature, it can be seen that for the sample there are the sharp peaks with 2θ values of 25.4°, 38.0° corresponding to (101), (004) crystal planes of anatase phase and the two typical peaks with 2θ values of 27.5°, 36.2° corresponding to (110), (101) crystal planes of rutile phase, respectively [14, 15]. On the other hand, the sample treated with ultrasound begins to appear rutile structure from more than 700 °C. Thus, the thermal stability of the sample treated with ultrasound increased than that of the sample treated without ultrasound. As shown in XRD, the peaks of treated TiO_2 nanoparticles become broader than that of pure rutile TiO_2 nanoparticles, because the ultrasound treatment can cause the homogeneous formation of a large number of seed nuclei, which leads to a smaller particle size [16].

The SEM and TEM images of the samples treated with and without ultrasound shown in Fig. 2 for comparing the differences and the changes between both of them. The TiO_2 powder is consisted of primary particles and secondary particles. The microsized secondary particles become accomplished with nanosized primary particles. The primary particle size of the sample treated without ultrasound is 5–15 nm (Fig. 2a), but that of the sample treated with ultrasound is only 3–6 nm (Fig. 2b). The particle size was in good agreement with the calculated value from XRD peaks (Table 1). Also, the secondary particle size of the sample treated without ultrasound is about 3 μm and that of the sample treated with ultrasound is about 2 μm. It can be known by particle size analyzer (Fig. 3). The samples treated without ultrasound happen a lot of interparticle agglomeration, but the samples treated with ultrasound do not happen interparticle agglomeration and particles are distributed uniformly.

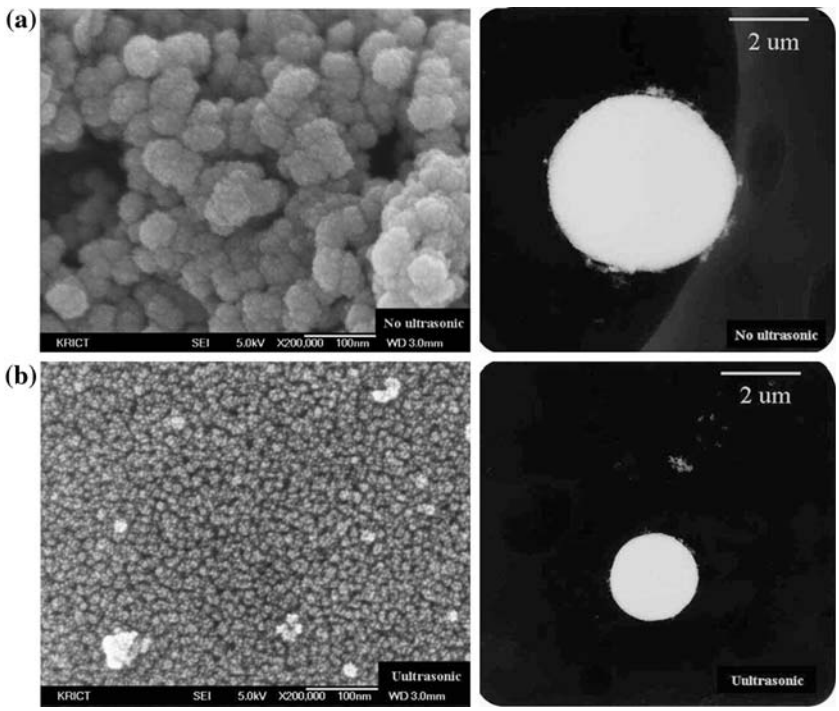

Fig. 2 FE-SEM and EF-TEM image for the as-prepared samples calcined at 600 °C for 2 h: without ultrasonic treatment (**a**), with ultrasonic treatment (**b**)

Table 1 Physical properties of prepared TiO_2 nanoparticles (SY–x–y, x: ultrasound treatment (1:without, 2:with), y: temperature)

Sample	Mean particle size[a] (nm)	Mean particle size[b] (nm)	Average pore size[c] (nm)	k_{app}[d] $\times 10^{-3}$ (min^{-1})
SY-1-Fresh	–	–	8.8	9.01
SY-1-400	8	9	10	10.61
SY-1-500	12	11	10.2	11.15
SY-1-600	15	13	11.4	8.48
SY-1-700	19	20	11.5	7.49
SY-1-800	38	35	12.3	6.55
SY-2-Fresh	–	–	10.8	9.49
SY-2-400	5	3	15.1	13.82
SY-2-500	6	5	15.1	15.06
SY-2-600	8	5	16.1	12.81
SY-2-700	14	13	17.5	7.83
SY-2-800	26	24	19.4	7.2

[a] Determined from the corresponding X-ray spectral peaks by the Scherrer equation of XRD

[b] Obtained by SEM

[c] Calculated from the nitrogen isotherm by the BJH method

[d] The apparent first order rate constants calculated by MB photocatalysis

The nitrogen adsorption-desorption isotherm of material obtained under different conditions indicates mesoporous structure, as seen in Fig. 4. The isotherm is of type IV, characteristic of mesoporous material [17]. These structures are the result of the formation of pores between TiO_2 nanoparticles [18, 19]. The hysteresis loop observed with the isotherm was mainly type H1, which is characterized by agglomerates of approximately uniform size, giving rise to a narrow pore size distribution. The sharp decline in the desorption curve is indicative of mesoporosity. At 500 °C, the pore size distribution calculated from desorption branch of the nitrogen isotherm by the BJH method reveals the average pore size of the sample treated without ultrasound of 10.2 nm and the average pore size of the sample treated with ultrasound of 15.1 nm. Figure 5 shows the effects of ultrasound treatment on the physical properties of the as-prepared samples. It could be seen from Fig. 5 that the sample prepared by ultrasound method showed a large specific surface area, and its values reached 155.7 m^2/g. With increasing calcinations temperature, the specific surface areas steadily decreased due to progressive aggregation of small crystallites into larger particles. The specific surface area of the sample treated without ultrasound began to decrease rapidly at 500 °C and the sample treated with ultrasound at 600 °C. Whereas, the average pore size of the sample treated without ultrasound began to increase dramatically at 500 °C and the sample treated with ultrasound at 600 °C. This was probably due to the fact that its phase structure appeared rutile. These results have a thread of connection with XRD results.

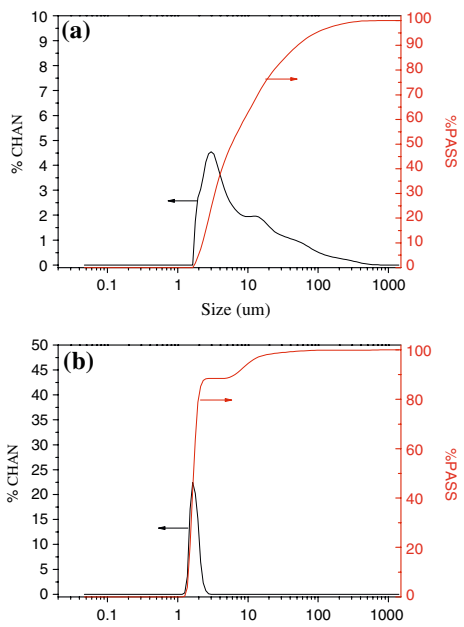

Fig. 3 Particle size distribution of the as-prepared samples calcined at 600 °C for 2 h: without ultrasonic treatment (**a**), with ultrasonic treatment (**b**)

The degradation of MB as a model reaction was studied to investigate the photocatalytic activities of as-prepared samples under UV irradiation. The changes in the concentration of MB recorded during UV irradiation at specific time intervals are shown in Fig. 6. Most of our experiments were run at an initial MB concentration of 0.05 mM, at which adequate color changes (hypsochromic effect) of the TiO_2 particle surface resulting from photocatalytic degradation of MB were observed. Control experiment shows that MB is not degraded in the dark or under UV light in the absence of catalysts for 1.5 h. It can be seen that the conversion of MB was higher when UV-light irradiation was applied in the presence of TiO_2 nanoparticles. In Fig. 6a, after exposure by UV light for 360 min, the degradation ratio of MB over the as-prepared samples treated without ultrasound is above 71%, with increasing calcinations temperatures, the degradation ratio of MB increases and reaches the maximum value of 91% at

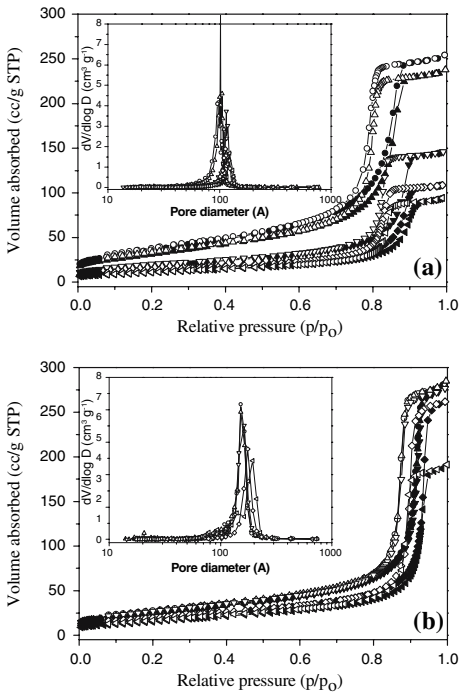

Fig. 4 The nitrogen adsorption-desorption isotherm and pore size distribution of the as-prepared samples calcined at 400 °C for 2 h (○), at 500 °C for 2 h (Δ), at 600 °C for 2 h (▽), at 700 °C for 2 h (◇), at 800 °C for 2 h (◁), respectively: without ultrasonic treatment (a), with ultrasonic treatment (b)

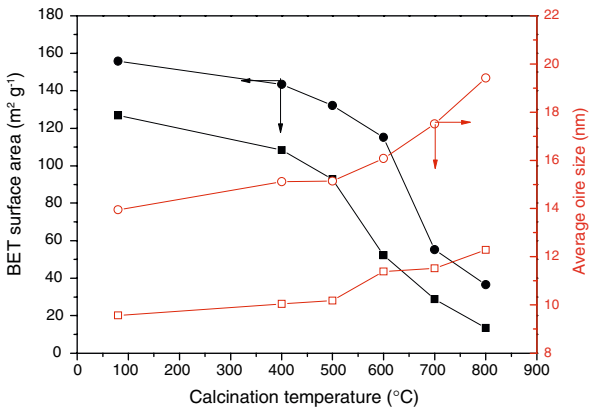

Fig. 5 The BET surface area and average pore size of the as-prepared samples calcined at different temperature under flowing air: without ultrasonic treatment (■, □), with ultrasonic treatment (●, ○)

calcinations temperature of 500 °C, and then decreases with increasing calcinations temperature successively. On the other hand, the degradation ratio of MB over the as-prepared samples treated with ultrasound is above 71%, with increasing calcinations temperatures, the degradation ratio of MB increases and reaches the maximum value of nearly 100% at calcinations temperature of 600 °C. The increase in photocatalytic activity is due to the formation of

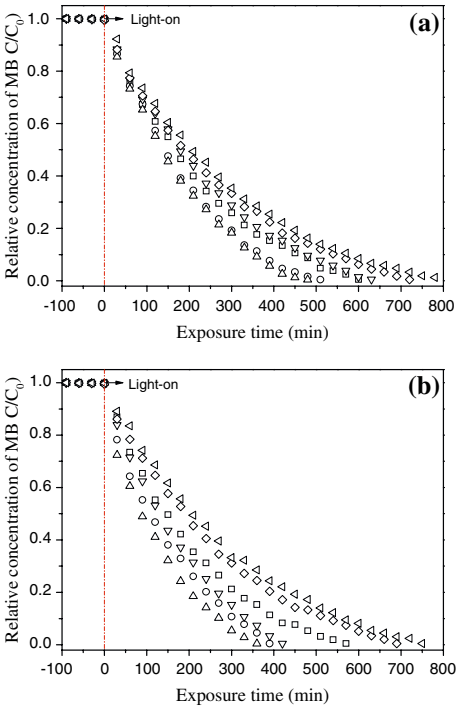

Fig. 6 Photodegradation of MB solution in the as-prepared fresh sample (□) and the as-prepared samples calcined at 400 °C for 2 h (○), at 500 °C for 2 h (Δ), at 600 °C for 2 h (▽), at 700 °C for 2 h (◇), at 800 °C for 2 h (◁), respectively: without ultrasonic treatment (a), with ultrasonic treatment (b)

anatase and the improvement of crystallization of anatase in the samples, while the decrease in the photocatalytic activity of TiO_2 powders calcined at above 500 °C and 600 °C, respectively, is due to the phase transformation of anatase to rutile and the growth of TiO_2 crystallites [20]. It also can be seen from Fig. 6, during the first 200 min of UV illumination the degradation ratio of MB by the TiO_2 nanocrystallites increases fastly, but after that the degradation ratio increases slowly. Under light-rich conditions, photocatalytic reaction rate depends on the adsorptive property of MB onto the catalysts surface. The more the amount of MB adsorbed onto the catalysts surface, the higher the photobleaching rate [21]. As the illumination time increasing, the amount of dye adsorbed onto the catalysts surface becomes smaller due to the photobleaching of MB by the catalysts [22]. Therefore, the degradation ratio of MB increases slowly after the first 200 min.

The plots of Fig. 6 provide a comparison between samples treated with and without ultrasound. On the basis of the results, the photocatalytic activity is the highest at 500 °C, but in case of samples treated without ultrasound, the photocataly activity of the sample treated without ultrasound began to decrease rapidly at 500 °C and the sample treated with ultrasound at 600 °C.

At present, although the detailed pathway of MB degradation reaction are not yet clear this study demonstrated that MB could be degraded largely over the photocatalysts under UV light irradiation.

The experimental data demonstrated that the photobleaching of MB by all samples followed the pseudo-first-order kinetics with respect to MB concentration. In general, external mass transfer is characterized by the initial solute uptake and can be calculated from the slope of plot of C/C_0 versus time. In analyzing the kinetic data of photocatalytic oxidations, mediated by photo-activated semiconductor particles, the data were fitted to the simple rate expression of the Langmuir–Hinshelwood (L–H) form as follows (Eq. 3):

$$R = -\frac{dC}{dt} = \frac{K_{Ad}kC_0}{1 + K_{Ad}C_0} \quad (1)$$

where C_0, K_{Ad} and k are the initial concentration of MB, the adsorption coefficient and the reaction rate constant respectively. The integration of Eq. 3 yields Eq. 4 as follows:

$$t = \frac{1}{K_{Ad}k} In\left(\frac{C_0}{C}\right) + \frac{1}{k}(C_0 - C) \quad (2)$$

The integrated form of Eq. 3 for a low initial concentration of MB of this study can be written as follows (Eq. 5):

$$In\left(\frac{C}{C_0}\right) = -K_{Ad}kt = -k_{app}t \quad (3)$$

where k_{app} is the apparent reaction rate constant and t is the reaction time.

Rate constant k_{app} has been chosen as the basic kinetic parameter for different systems, since it is independent of used concentration [23, 24].

The apparent first order rate constants (k_{app}) for the prepared photocatalysts are shown in Fig. 7. As can be seen from the figure, the degradation rate is faster for samples treated with ultrasound than for samples treated without ultrasound. With increasing calcinations temperature, the k obviously increased. The maximum k_{app} value of the sample treated without ultrasound was reached at 500 °C and its value was 0.011 min^{-1}, while that of the sample treated with ultrasound was reached at 600 °C and its value was 0.015 min^{-1}. The high photocatalytic activity of the sample treated with ultrasound is due to its relative large specific surface areas, small particle size and good crystallization. On the other hand, at a higher temperature, the apparent first order rate constants decrease rapidly and reach a minimum value of 0.007 at 800 °C due to drastic decrease in specific surface areas and increase particle size and rutile contents.

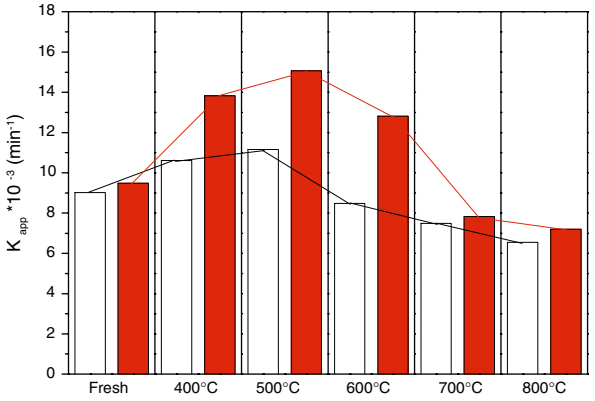

Fig. 7 The dependence of the apparent first order rate constants (k_{app}) on calcinations temperature under flowing air: without ultrasonic treatment (□), with ultrasonic treatment (■)

4 Conclusions

TiO_2 nanoparticles were prepared by hydrolysis using $TiCl_4$ in a mixed solvent of iso-propyl alcohol and water with ultrasound treatment. The specific surface area, thermal stability and crystallization of the as-prepared samples treated with ultrasound were higher than those of samples treated without ultrasound. This may be ascribed to the fact that ultrasound treatment enhances hydrolysis of $TiCl_4$ and crystallization of TiO_2 gel.

The photocatalytic degradation of a aqueous solution of methylene blue shows a remarkable increase when it is carried out in the presence of ultrasound. With increasing calcinations temperatures, the degradation ratio of MB increases and reaches the maximum value of nearly 100%, and then decreases. The photocatalytic activities were ultimately evaluated by the rate constant k_{app} for MB decomposition reaction, which was determined from the linear relation between the logarithm of relative concentration of MB and irradiation time. The photobleaching of MB by all samples followed the pseudo-first-order kinetics with respect to MB concentration. The photocatalytic activity is the highest at 500 °C, but in case of samples treated without ultrasound, the photocatalytic activity of the sample treated without ultrasound began to decrease rapidly at 500 °C and the sample treated with ultrasound at 600 °C. Also, from same condition, the activity of samples treated with ultrasound was higher than that of samples treated without ultrasound.

References

1. Guo W, Lin Z, Wang X, Song G (2003) Microelectron Eng 66:95
2. Piwonski I, Ilik A (2006) Appl Surf Sci 253:2835
3. Sandell A, Andersson MP, Johansson MK, Karlsson PG, Alfredsson Y, Schnadt J, Siegbahn H, Uvdal P (2003) Surf Sci 530:63

4. Xia B, Huang H, Xie Y (1999) Mat Sci Eng B 57:150
5. Ryu YB, Lee GD, Hong SS (2006) J Ind Eng Chem 12:289
6. JC Yu, Tang HY, Yu J, Chan HC, Zhang L, Xie Y, Wang H, Wong SP (2002) J Photochem Photobiol A 153:211
7. Qian Y, Chen Q, Chen Z, fan C, Zhou G (1993) J Mater Chem 3:203
8. Yu J, Zhou M, Cheng B, Yu H, Zhao X (2005) J Mol Catal A Chemical 227:75
9. Awati PS, Awate SV, Shah PP, Ramaswamy V (2003) Catal Commun 4:393
10. Suslick KS, Price GJ (1999) Annu Rev Mater Sci 29:295
11. Spurr RA, Myers H (1957) Anal Chem 24:760
12. Tang J, Zou Z, Yin J, Ye J (2003) Chem Phys Lett 382:175
13. Li FB, Li XZ (2002) Appl Catal A 228:15
14. Kim SY, Chang TS, Lee DK, Shin CH (2005) J Ind Eng Chem 11:194
15. Li Y, Liu J, Jia Z (2006) Mater Lett 60:1753
16. Huang WP, Tang XH, Wang YQ, Koltypin Y, Gedanken A (2000) Chem Commun 20:1415
17. Zhang Y, Zhang H, Xu Y, Wang Y (2004) J Solid State Chem 177:3490
18. Yu JC, Yu JG, Zhang LZ, Ho WK (2002) J Photochem Photobiol A 148:263
19. Hung W, Tang X, Wang Y, Koltypin Y, Gedanken A (2000) Chem Commun 15:1415
20. Yu JG, Yu HG, Cheng B, Zhao XJ, Yu JC, Ho WK (2003) J Phys Chem B 107:13871
21. Miyauchi M, Ikezawa A, Tobimatsu H, Irie H, Hashimoto K (2004) Phys Chem Chem Phys 6:865
22. Miyauchi M, Nakajima A, Watanabe T, Hashimoto K (2002) Chem Mater 14:4714
23. Matos J, Laine J, Herrmann JM (1998) Appl Catal B 18:281
24. Qourzal S, Assabbane A, Aic-Ichou Y (2004) J Photochem Photobiol A Chem 163:317